Spin-singlet topological superconductivity in the attractive Rashba-Hubbard model

Peter Doak,[1] Giovanni Balduzzi,[2] Pontus Laurell,[3] Elbio Dagotto,[3,4] and Thomas A. Maier[1]
[1]*Computational Sciences and Engineering Division, Oak Ridge National Laboratory, Oak Ridge, Tennessee 37831, USA*
[2]*Institute for Theoretical Physics, ETH Zurich, 8093 Zurich, Switzerland*
[3]*Department of Physics and Astronomy, University of Tennessee, Knoxville, Tennessee 37996, USA*
[4]*Materials Science and Technology Division, Oak Ridge National Laboratory, Oak Ridge, Tennessee 37831, USA*

(Received 22 November 2022; revised 25 April 2023; accepted 22 May 2023; published 1 June 2023)

Fully gapped, spin-singlet superconductors with antisymmetric spin-orbit coupling in a Zeeman magnetic field provide a promising route to realize superconducting states with non-Abelian topological order and therefore fault-tolerant quantum computation. Here we use a quantum Monte Carlo dynamical cluster approximation to study the superconducting properties of a doped two-dimensional attractive Hubbard model with Rashba spin-orbit coupling in a Zeeman magnetic field. We generally find that the Rashba coupling has a beneficial effect towards *s*-wave superconductivity. In the presence of a finite Zeeman field, when superconductivity is suppressed by Pauli pair breaking, the Rashba coupling counteracts the spin imbalance created by the Zeeman field by mixing the spins, and thus restores superconductivity at finite temperatures. We show that this favorable effect of the spin-orbit coupling is traced to a spin-flip driven enhancement of the amplitude for the propagation of a pair of electrons in time-reversed states. Moreover, by inspecting the Fermi surface of the interacting model, we show that for sufficiently large Rashba coupling and Zeeman field, the superconducting state is expected to be topologically nontrivial.

DOI: 10.1103/PhysRevB.107.224501

I. INTRODUCTION

In topological superconductors, the nontrivial topology of the bulk electronic structure leads to the emergence of Majorana bound states within the bulk superconducting gap [1–3]. These quasiparticles may be used for fault-tolerant quantum computing [4], and the search for new topological superconductors that host robust Majorana modes has therefore been an important priority but also a central challenge in quantum materials research. While topological superconductivity is usually associated with odd-parity spin triplet pairing, it was shown that spin-singlet, even parity superconductors can also host a non-Abelian topological phase in the presence of spin-orbit coupling and a Zeeman magnetic field [5,6]. Experimental platforms to realize such a system include heterostructures of a semiconducting thin film sandwiched between an *s*-wave superconductor and a ferromagnetic insulator [7], a two-dimensional electron gas adjacent to an interdigitated superconductor/ferromagnet structure [8], electric double layer transistors with an *s*-wave superconductor/ferromagnet heterostructure [9], and superfluids of cold atoms [5,10].

Realizing topological superconductivity requires an intricate cooperation between helical states created by spin-orbital coupling, time-reversal symmetry breaking, and superconductivity. Most studies of these ingredients, however, have used Bogoliubov-de-Gennes (BdG) weak-coupling mean-field theory [5,11–13], which assumes that superconductivity is present and unaffected by the correlations, the spin-orbit coupling, or the Zeeman field. However, in order to provide general guiding principles for the design of topological superconducting materials, the effects of correlations, spin-orbit coupling, and magnetic fields have to be treated on the same footing on a microscopic, beyond weak-coupling mean-field level, in order to properly assess the interplay between strong correlations and topology. Such work, however, is scarce, with only a few exceptions that include the dynamical mean-field theory (DMFT) work by Nagai *et al.* [9] and Lu *et al.* [14]. Here we investigate these effects and the feedback between them on a microscopic level within numerical quantum Monte Carlo (QMC) dynamical cluster approximation (DCA) calculations of a Rashba-Hubbard model using a large enough cluster that properly accounts for the effects of the nonlocal Rashba coupling. We also use additional density matrix renormalization group (DMRG) calculations on a two-leg ladder (reported in Appendix B) to show that our DCA results are robust. Here we consider an out-of-plane Zeeman field. Systems with in-plane magnetic field were considered in Refs. [15,16].

II. MODEL AND METHODS

We consider a two-dimensional square lattice attractive Rashba-Hubbard model in a Zeeman magnetic field. Its Hamiltonian is given by

$$H = \sum_{\mathbf{k}} \psi^{\dagger}_{\mathbf{k}} (\epsilon_{\mathbf{k}} \mathbb{1} - h\sigma_3 + 2\lambda_{\mathrm{SOC}}\, \boldsymbol{\sigma} \cdot \mathbf{g}_{\mathbf{k}}) \psi_{\mathbf{k}} + U \sum_i n_{i\uparrow} n_{i\downarrow}. \tag{1}$$

Here, we have used a spinor notation $\psi^{\dagger}_{\mathbf{k}} = (c^{\dagger}_{\mathbf{k}\uparrow}, c^{\dagger}_{\mathbf{k}\downarrow})$, with $c^{\dagger}_{\mathbf{k}\sigma}$ creating an electron with wave vector $\mathbf{k}$ and spin $\sigma = \uparrow, \downarrow$. For the square lattice with only nearest-neighbor hopping t, which we use as the energy unit ($t = 1$), the energy dispersion is $\epsilon_{\mathbf{k}} = -2t(\cos k_x + \cos k_y)$. $\boldsymbol{\sigma} = (\sigma_1, \sigma_2, \sigma_3)$ are

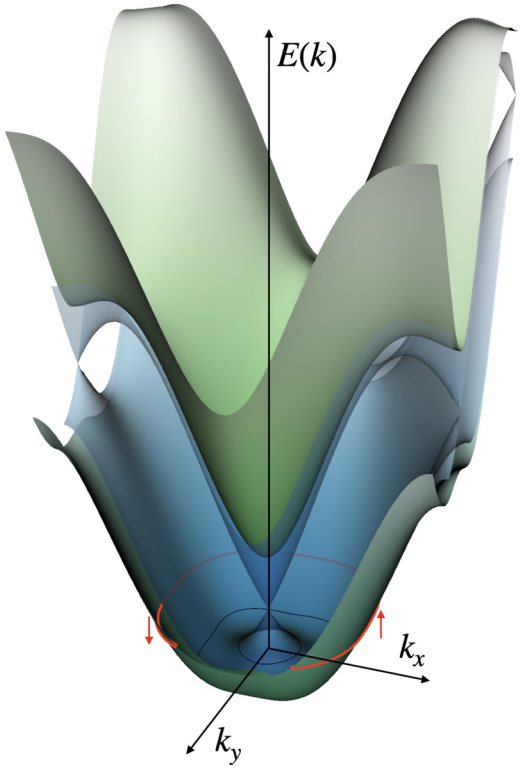

FIG. 1. Illustration of the bandstructure with Rashba spin-orbit coupling and Zeeman field. In the presence of finite Rashba spin-orbit coupling λ_{SOC}, the Kramers degenerate bands for spin $\uparrow$ and $\downarrow$ split into two pseudospin bands, resulting in a Dirac cone near the Γ point where the two bands touch (blue band structure). When the Zeeman field breaks time-reversal symmetry, a gap opens at Γ (green band structure) resulting in a single ("spinless") Fermi surface (red line) when the chemical potential is tuned to an energy within the gap.

the Pauli matrices, h the Zeeman magnetic field, and λ_{SOC} the Rashba spin-orbit coupling with $g_{\mathbf{k}} = (-\sin k_y, \sin k_x, 0)$. The second part of the Hamiltonian describes the on-site attractive interaction $U < 0$ with the density operators $n_{i\sigma} = c^{\dagger}_{i\sigma} c_{i\sigma}$. Here we have set $U = -4t$ and the electron density $\langle n \rangle = 0.25$. We note that orbital effects of the magnetic field are ignored in this Hamiltonian. Our results are therefore more relevant to systems in which these effects are expected to not be important, such as, e.g., strongly correlated systems or ultracold charge neutral fermionic atoms [6]. In addition, it was argued that in heterostructures of a semiconducting thin film sandwiched between a ferromagnetic insulator and an s-wave superconductor [7], the Zeeman field primarily arises from electron tunneling and not the magnetic field generated by the ferromagnetic insulator, justifying the neglect of orbital effects of the magnetic field for such systems [3]. Other systems consisting of a Tl-Pb monolayer on a Si(111) substrate and an ion gel, s-wave superconductor, ferromagnet heterostructure were also proposed in Ref. [9] as a possible realization of the physics described by this Hamiltonian.

The band structure $E(\mathbf{k})$ that results from diagonalizing the noninteracting part of the Hamiltonian is schematically illustrated in Fig. 1. In the presence of a finite spin-orbit coupling λ_{SOC} but zero Zeeman field, the band structure splits into two pseudospin bands that are degenerate only at the Γ point ($\mathbf{k} = 0$), resulting in a Dirac cone (blue surface). The Fermi surface always has two sheets, no matter where the chemical potential is located. For finite Zeeman field h, a gap opens at Γ (green surface). In this case, when the chemical potential μ is tuned to fall within the gap, the Fermi surface consists of only a single (pseudospin) sheet with a helical spin structure, where the physical electron spin is pointing in opposite directions on opposite sides of the Fermi surface due to the spin-momentum locking induced by the spin-orbit coupling. This allows for the formation of spin-singlet Cooper pairs with opposite momenta $\mathbf{k}, \uparrow$ and $-\mathbf{k}, \downarrow$ in the presence of an attractive interaction. However, the pairing in this case is effectively spinless, since the other pseudospin degree of freedom is gapped out, and the superconducting state is expected to be topologically nontrivial. We note that while this pairing state is a spin-singlet pairing state in the original spin basis, it corresponds to a spin-triplet state in the pseudospin basis. In fact, Sato *et al.* have shown that the s-wave BdG Hamiltonian can be mapped to a spinless chiral p-wave superconductor in the chiral pseudospin basis [6].

In principle, the topological character of the superconducting phase of the model in Eq. (1) is to be determined by calculating the Thouless-Kohmoto-Nightingale-Nijs (TKNN) invariant [6]. However, the calculation of topological invariants for interacting systems is more difficult than for noninteracting systems and would involve calculations inside the superconducting phase and an additional analytic continuation of the imaginary time quantum Monte Carlo data to real frequency to construct the zero frequency single-particle Green's function, from which an effective Hamiltonian can be defined [14]. We therefore resorted to the method introduced by Sato *et al.* [6] for Rashba superconductors relating the TKNN invariant to the winding number defined as the xy-plane spin rotation on the Fermi surface. Specifically, we use the argument by Nagai *et al.* [9] that a superconducting state below T_c with nontrivial topological character is associated with a nonzero winding number on the normal state Fermi surface just above T_c. Consistent with the argument presented above, the winding number is nonzero when only a single nondegenerate Fermi surface sheet is present.

Here we use nonperturbative QMC/DCA [17–19] calculations for the model in Eq. (1) to study whether this physics can indeed be realized and to determine the superconducting transition temperature T_c in the presence of both finite Rashba spin-orbit coupling λ_{SOC} and Zeeman field h. In the absence of these terms, the attractive Hubbard model in Eq. (1) has been studied extensively over the past several decades [20–30]. Away from half-filling $\langle n \rangle = 1$, this model has a finite-temperature Kosterlitz-Thouless s-wave superconducting transition that can be mapped out essentially exactly as QMC does not face a Fermion sign problem for this model [26,29,30].

When λ_{SOC} is finite but $h = 0$, the model preserves time-reversal symmetry. In this case, there is still no sign problem in the QMC [31]. For $|h| > 0$, however, time reversal symmetry is broken, and the QMC calculations are not protected by symmetry from a sign problem (in this case a phase problem since the Hamiltonian is complex). The model with finite λ_{SOC} and h was studied with single-site DMFT by Nagai *et al.* in

Ref. [9]. The single-site calculation is sign-problem free, but the purely nonlocal Rashba spin-orbit coupling vanishes in the effective single-site DMFT problem and is therefore not adequately treated in the calculation. Here, to properly take into account the effects of the Rashba coupling, we use an eight-site cluster for the DCA calculations and a continuous-time auxiliary-field QMC algorithm [32,33] to solve the effective cluster problem as implemented in the DCA++ code [34]. The eight-site cluster is the smallest cluster for which the $\lambda_{\rm SOC}$ coupling does not vanish for the effective cluster problem. For the parameters of interest in this work, we do not find a strong phase problem for this cluster, allowing us to perform simulations for very low temperatures and accurately study the effects of $\lambda_{\rm SOC}$ and h on the superconducting properties of the model.

In order to do so, we calculate the s-wave pair-field susceptibility,

$$P_s(T) = \int_0^\beta d\tau \langle \mathcal{T}_\tau \Delta_s(\tau)\Delta_s^\dagger(0)\rangle, \tag{2}$$

with $\Delta_s^\dagger = 1/\sqrt{N}\sum_{\mathbf{k}} c^\dagger_{\mathbf{k}\uparrow}c^\dagger_{-\mathbf{k}\downarrow}$. The calculation of $P_s(T)$ within the DCA method is described in detail in Appendix A. T_c is determined as the temperature T at which $P_s(T)$ diverges, or equivalently, $1/P_s(T)$ becomes zero (see Fig. 6 in Appendix A). We will also study its leading order term, the intrinsic pair-field susceptibility $P_{s,0}(T)$, which reflects the amplitude for the propagation of a pair of electrons in time-reversed momentum and spin states, in order to get insight into the pairing behavior. This quantity is given by

$$P_{s,0} = \frac{T}{N}\sum_k [G_{\uparrow\uparrow}(k)G_{\downarrow\downarrow}(-k) - G_{\uparrow\downarrow}(k)G_{\downarrow\uparrow}(-k)]. \tag{3}$$

Here we have used the notation $k = (\mathbf{k}, i\omega_n)$ for fermionic Matsubara frequencies $\omega_n = (2n+1)\pi T$ and $G_{\sigma\sigma'}(k)$ is the fully interacting Green's function for the model in Eq. (1). The first term is the usual term for spin-singlet $(\mathbf{k}\uparrow, -\mathbf{k}\downarrow)$ pairs. The second, spin-flip term $G_{\uparrow\downarrow}G_{\downarrow\uparrow}$ is only finite when the spin-orbit coupling $\lambda_{\rm SOC}$ mixes $\uparrow$ and $\downarrow$ spins, which leads to finite off-diagonal Green's function components $G_{\uparrow\downarrow}$ and $G_{\downarrow\uparrow}$.

III. RESULTS AND DISCUSSION

Figure 2 shows the superconducting transition temperature T_c versus the Rashba spin-orbit coupling $\lambda_{\rm SOC}$ for different values of the Zeeman magnetic field h. T_c was obtained as the temperature at which the s-wave pair-field susceptibility $P_s(T)$ diverges (see Fig. 6 in Appendix A). We find nonmonotonic behavior for $h = 0$ and $0.5t$, while for $h = t$, T_c monotonically increases up to the largest $\lambda_{\rm SOC}$ we have studied. For $h = 0$ and $\lambda_{\rm SOC} = 0$, $T_c \approx 0.11t$ and increases by about 20% to $T_c \sim 0.13t$ at $\lambda_{\rm SOC} \approx 0.4t$ before it decreases at larger $\lambda_{\rm SOC}$. This initial increase in T_c with $\lambda_{\rm SOC}$ is also found for finite h. In this case, when $\lambda_{\rm SOC} = 0$, superconductivity is suppressed for fields larger than the upper critical field due to Pauli pair breaking. For $h = 0.5t$ (t), we do not find a superconducting transition for $\lambda_{\rm SOC} = 0$ (0 and 0.125t). For larger $\lambda_{\rm SOC}$, however, superconductivity is restored and T_c initially increases with $\lambda_{\rm SOC}$ before it decreases at larger $\lambda_{\rm SOC}$. This behavior is

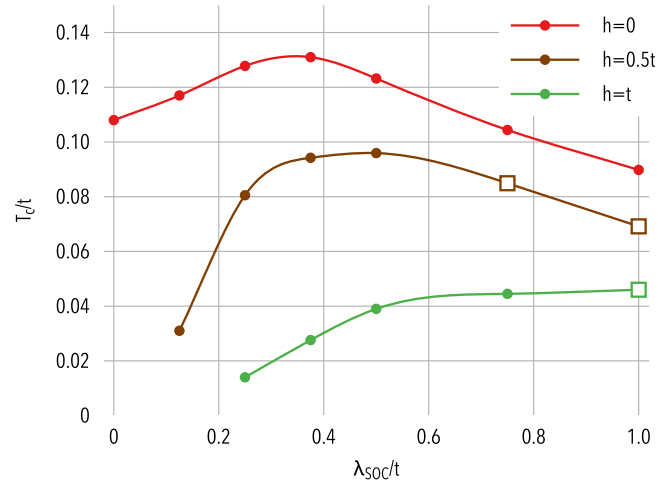

FIG. 2. Superconducting transition in the attractive Rashba-Hubbard model. The superconducting transition temperature T_c versus Rashba spin-orbit coupling $\lambda_{\rm SOC}$ for different Zeeman magnetic fields h. The data points with square symbols indicate the parameters for which the superconducting state is expected to be topologically nontrivial based on the results for the Fermi surface shown in Fig. 4. Results are shown for an electron filling $\langle n\rangle = 0.25$ and $U = -4t$, and the DCA calculations were performed for an eight-site cluster.

consistent with our DMRG calculations of a two-leg Rashba-Hubbard ladder as reported in Appendix B, where we find that the binding energy for a pair of holes is negative and has a minimum at intermediate Rashba coupling for finite Zeeman fields. The DMRG calculations also show nonmonotonic behavior in the $\lambda_{\rm SOC}$ dependence of the on-site pair-pair correlations with a pronounced enhancement for intermediate Rashba coupling. Our results are also consistent with those found previously in single-site DMFT calculations for this model [9] and note that, as shown in that work, mean-field theory does not capture the nonmonotonic behavior. For the data points with the square symbols at large $\lambda_{\rm SOC}$ and finite h, we expect the superconducting state to be topologically nontrivial, based on results for the normal state Fermi surface, as we will discuss later. For $h = 0.5t$ and $\lambda_{\rm SOC} = 0.75t$, the T_c of this topological state is only reduced by about 20% to that of the topologically trivial state for $h = \lambda_{\rm SOC} = 0$ from $T_c \approx 0.11t$ to $T_c \approx 0.085t$.

From Fig. 2 it is clear that $\lambda_{\rm SOC}$ increases the Pauli-limit upper critical field above which superconductivity is suppressed, and thus restores superconductivity for fields above the upper critical field of the system with $\lambda_{\rm SOC} = 0$. We now discuss results for the intrinsic s-wave pair-field susceptibility $P_{s,0}$ defined in Eq. (3) in order to provide insight into this behavior. In Fig. 3, we show results for the temperature and $\lambda_{\rm SOC}$ dependence of $P_{s,0}$. In conventional (BCS) theory, this quantity has a logarithmic (Cooper) divergence as $T \to 0$, so that any attractive interaction, no matter how weak, leads to a superconducting transition at finite temperature. In an unconventional superconductor, however, the physics can be different. In the cuprate pseudogap phase, for example, this Cooper instability is absent, and the superconducting transition is driven by an effective interaction that increases

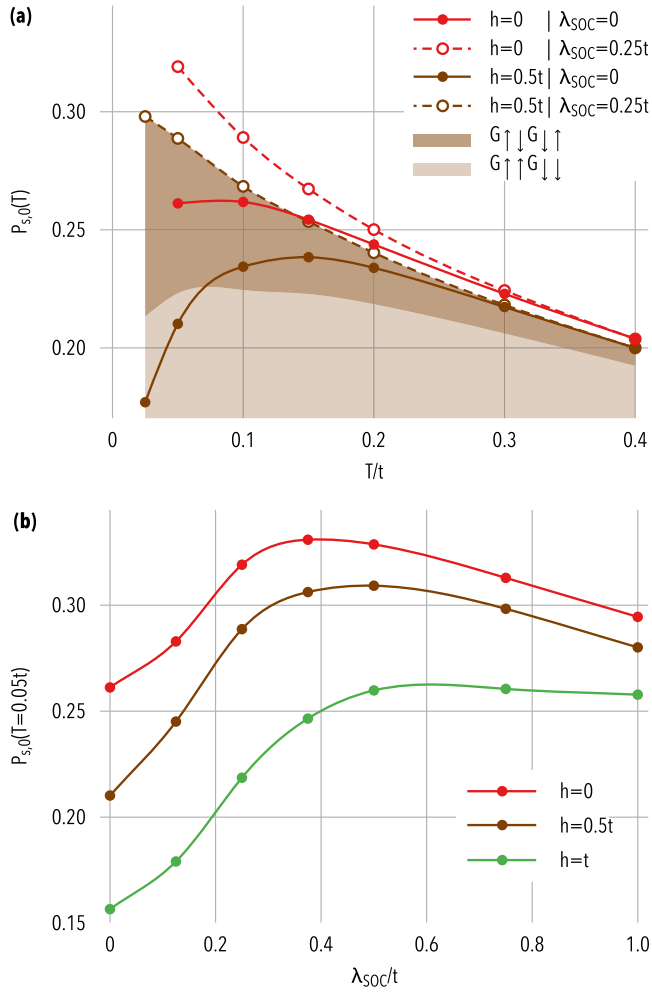

FIG. 3. Intrinsic pair-field susceptibility. (a) Temperature dependence of the s-wave intrinsic pair-field susceptibility $P_{s,0}(T)$ for different Zeeman fields h and Rashba couplings $\lambda_{\rm SOC}$. The light (dark) shaded regions show the contributions in Eq. (3) of the first $G_{\uparrow\uparrow}G_{\downarrow\downarrow}$ (second $G_{\uparrow\downarrow}G_{\downarrow\uparrow}$) terms to $P_{s,0}(T)$ for $h = 0.5$, $\lambda_{\rm SOC} = 0.25$. (b) $P_{s,0}(T)$ at fixed temperature $T = 0.05t$ versus $\lambda_{\rm SOC}$. All results are shown for an electron filling $\langle n\rangle = 0.25$ and $U = -4t$, and the DCA calculations were performed for an eight-site cluster.

with decreasing temperature [35]. Thus, a logarithmic divergence in $P_{s,0}(T)$ is a sufficient, but not necessary condition for a superconducting instability to occur.

Figure 3(a) plots the temperature T dependence of $P_{s,0}(T)$ for two different values of h and $\lambda_{\rm SOC}$. For $\lambda_{\rm SOC} = 0$ (solid circles), finite $h = 0.5t$ splits the Kramers degenerate Fermi surface into two ($\uparrow$ and $\downarrow$) sheets. As a result, there are no states available at $-\mathbf{k}$ on the $\downarrow$ sheet to pair with the $\mathbf{k}, \uparrow$ state. Consequently, $P_{s,0}(T)$ is significantly suppressed at low temperatures by the Zeeman field. A finite $\lambda_{\rm SOC}$ mixes spin $\uparrow$ with spin $\downarrow$ and thus counteracts the spin imbalance created by the h field. Consistent with this expectation, for $\lambda_{\rm SOC} = 0.25t$ (open cirlces), the low temperature behavior of $P_{s,0}(T)$ changes significantly, now showing a strong upturn with decreasing temperature even for $h > 0$, which eventually leads to the finite T_c shown in Fig. 2. Albeit less dramatic, this enhancement occurs even for $h = 0$ and is the reason for the enhancement of T_c with finite spin-orbit coupling $\lambda_{\rm SOC}$. For $h = 0.5t$ and $\lambda_{\rm SOC} = 0.25t$, the two terms, $G_{\uparrow\uparrow}G_{\downarrow\downarrow}$ and $G_{\uparrow\downarrow}G_{\downarrow\uparrow}$ that contribute to $P_{s,0}$ in Eq. (3) are shown as shaded regions. The standard $G_{\uparrow\uparrow}G_{\downarrow\downarrow}$ contribution remains suppressed at low temperatures, even in the presence of finite $\lambda_{\rm SOC}$. In contrast, the spin-flip $G_{\uparrow\downarrow}G_{\downarrow\uparrow}$ contribution keeps rising with decreasing temperature, leading to the low-temperature increase of $P_{s,0}(T)$ for finite $\lambda_{\rm SOC}$. The $\lambda_{\rm SOC}$ and h dependence of $P_{s,0}(T)$ at fixed $T = 0.05t$ in Fig. 3(b) closely tracks the $\lambda_{\rm SOC}$ dependence of T_c in Fig. 2, showing that it is indeed the effect of $\lambda_{\rm SOC}$ and h on the intrinsic pair-field susceptibility $P_{s,0}$ that determines T_c.

The key for understanding the different effects of $\lambda_{\rm SOC}$ and h on $P_{s,0}(T)$ is the Fermi surface and band structure plotted in Fig. 4. Here we show two different parameter sets: $h = 0.5t$, $\lambda_{\rm SOC} = 0.25t$ in Fig. 4(a) and $h = t$, $\lambda_{\rm SOC} = t$ in Fig. 4(b). The top two panels show $|\nabla_{\mathbf{k}} n^{\sigma}_{\mathbf{k}}|$ as a proxy for the Fermi surface, where $n^{\sigma}_{\mathbf{k}} = c^{\dagger}_{\mathbf{k}\sigma} c_{\mathbf{k}\sigma}$ is the occupation in momentum space for spin σ. The bottom panels show the band structure of the noninteracting model, but including the Hartree term of the self-energy, to serve as a leading order approximation of the interacting single-particle spectrum that can be compared with $|\nabla_{\mathbf{k}} n^{\sigma}_{\mathbf{k}}|$ in the top panels. As is clear from these plots, the Fermi level crossing of the bands and their spin σ weights are consistent with the Fermi surface plots in the top panels.

For the case with $h = 0.5t$, $\lambda_{\rm SOC} = 0.25t$ in Fig. 4(a), one sees two bands crossing the Fermi level and two Fermi surface sheets closed around the Γ point with very different spin weights. The spin-orbit induced admixture of the opposite spin, although weak, leads to a finite spin-flip $G_{\uparrow\downarrow}G_{\downarrow\uparrow}$ contribution to $P_{s,0}(T)$ that is immune to the field induced suppression at low temperature, thus restoring the superconducting instability.

For the second case with $h = t$, $\lambda_{\rm SOC} = t$ in Fig. 4(b), the situation is very different. The splitting of the bands is much larger resulting in a single Fermi surface sheet only. The states on this sheet have predominantly spin $\downarrow$ character, but now with a much larger admixture of spin $\uparrow$ electrons. For this case of a single sheet, the superconducting state is expected to be topologically nontrivial, since the pairing (in the chiral pseudospin basis) is effectively spinless due to the absence of the second Fermi surface sheet. As indicated by the square data points in Fig. 2, the cases with $h = 0.5t$ and $\lambda_{\rm SOC} \geqslant 0.75t$ are also expected to be topologically nontrivial based on their Fermi surface (not shown).

IV. SUMMARY AND CONCLUSIONS

We have used a dynamic cluster quantum Monte Carlo approximation to study s-wave superconductivity in the attractive Hubbard model in the presence of a Rashba spin-orbit coupling $\lambda_{\rm SOC}$ and a Zeeman magnetic field h for an electron filling $\langle n\rangle = 0.25$. Under certain conditions, these ingredients can lead to a spin-singlet superconducting state that is topologically nontrivial. We have found that a Rashba coupling with moderate strength $\lambda_{\rm SOC} \sim 0.5t$ has a beneficial effect towards superconductivity. By mixing spin $\uparrow$ with $\downarrow$ states, it counteracts the spin imbalance generated by the h field and thus creates $-\mathbf{k}_F, \downarrow$ Fermi level states that can pair with

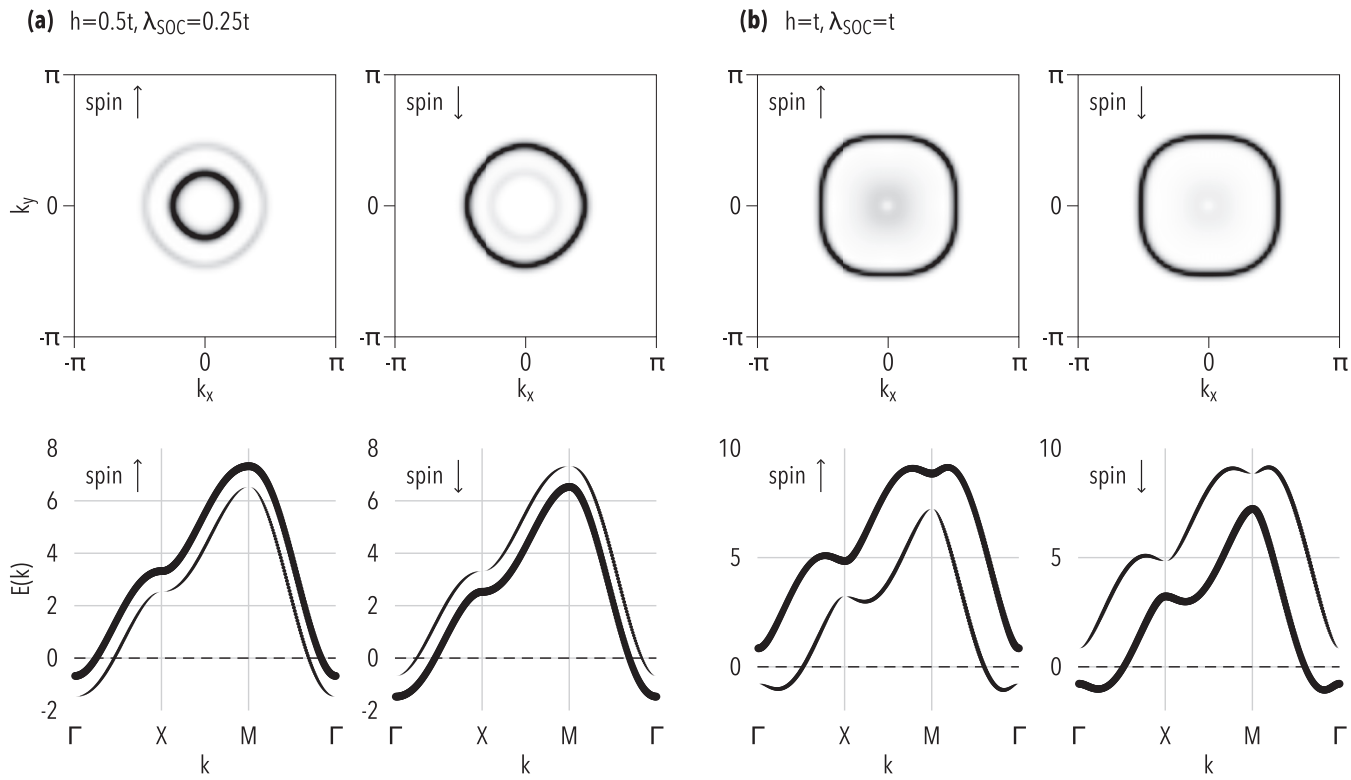

FIG. 4. Fermi surface and band structure. (Top panels) The gradient of the momentum space occupation, $|\nabla_k n(k)|$ for (a) $h = 0.5$, $\lambda_{\rm SOC} = 0.25$ and (b) $h = 1.0$, $\lambda_{\rm SOC} = 1.0$ for spin $\uparrow$ and $\downarrow$. (Bottom panels) Corresponding band structure in Hartree approximation with the weight of spin $\uparrow$ and $\downarrow$ indicated by line thickness.

degenerate $\mathbf{k}_F, \uparrow$ states. This promotes a superconducting transition for fields well above the Pauli limit upper critical field at $\lambda_{\rm SOC} = 0$. We show that this favorable effect of $\lambda_{\rm SOC}$ is traced to a spin-flip driven enhancement of the electron pair propagation amplitude $P_{s,0}$, which is induced by the spin mixture. Finally, we used the gradient of the momentum space occupation $n(\mathbf{k})$ to obtain information on the Fermi surface of the interacting system for different $\lambda_{\rm SOC}$ and h. For sufficiently large $\lambda_{\rm SOC}$ and h, we find that the Fermi level falls within the gap of the effective two-band system, and the Fermi surface consists of only a single (pseudospin) sheet. For this case, the superconducting state below T_c is effectively spinless and therefore expected to be topologically nontrivial. For the parameters we have studied, we find that the highest T_c for this topological state is only reduced by about 20% from the T_c of the topologically trivial state in the absence of spin-orbit coupling and magnetic field. These results give new insight into the effects of spin-orbit coupling and magnetic fields on the superconducting behavior of correlated electron systems, and thus provide general guidance on how to tune the relative strengths of these couplings in the search for new topological superconductors.

ACKNOWLEDGMENTS

We acknowledge useful discussions with Fakher Assaad. The work by T.A.M., E.D., and P.L. was supported by the U.S. Department of Energy, Office of Science, Basic Energy Sciences, Materials Sciences and Engineering Division. P.D. acknowledges support from the Laboratory Directed Research and Development Program of Oak Ridge National Laboratory, managed by UT-Battelle, LLC, for the U.S. Department of Energy. G.B. acknowledges support from the Scientific Discovery through Advanced Computing (SciDAC) program funded by the U.S. Department of Energy, Office of Science, Advanced Scientific Computing Research and Basic Energy Sciences, Division of Materials Sciences and Engineering for code development. An award of computer time was provided by the INCITE program. This research also used resources of the Oak Ridge Leadership Computing Facility, which is a DOE Office of Science User Facility supported under Contract No. DE-AC05-00OR22725. This manuscript has been authored by UT-Battelle, LLC, under Contract No. DE-AC0500OR22725 with the U.S. Department of Energy. The United States Government retains and the publisher, by accepting the article for publication, acknowledges that the United States Government retains a nonexclusive, paid-up, irrevocable, worldwide license to publish or reproduce the published form of this manuscript, or allow others to do so, for United States Government purposes. The Department of Energy will provide public access to these results of federally sponsored research in accordance with the DOE Public Access Plan.

APPENDIX A: DCA CALCULATION OF THE *s*-WAVE PAIR-FIELD SUSCEPTIBILITY

In order to calculate the *s*-wave pair-field susceptibility [Eq. (2) in the main text] for the model in Eq. (1), we follow the usual DCA formalism described in Refs. [18,36] to

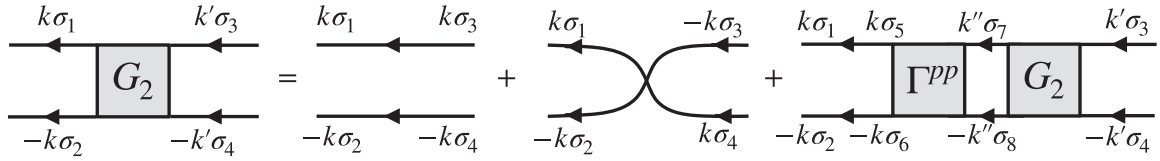

FIG. 5. Diagrams for the Bethe-Salpeter equation in the particle-particle channel. For finite (spin-mixing) Rashba coupling, an additional diagram with crossing Green's function legs contributes in leading order. This diagram gives rise to the enhancement of s-wave pair correlations found at low temperatures.

calculate susceptibilities for the lattice in the thermodynamic limit. This requires a calculation of the four-point two-particle Green's function,

$$G_{2,\sigma_1\ldots\sigma_4}(x_1,x_2;x_3,x_4) = \left\langle T_\tau c_{\sigma_1}(x_1)c_{\sigma_2}(x_2)c^\dagger_{\sigma_3}(x_3)c^\dagger_{\sigma_4}(x_4)\right\rangle, \tag{A1}$$

where the combined index $x_i = (\mathbf{x}_i, \tau_i)$ has both spatial $\mathbf{x}_i$, and imaginary time τ_i coordinates. Fourier transforming on both the space and time variables gives $G_{2,\sigma_1\ldots\sigma_4}(k_1,k_2;k_3,k_4)$ with $k_\ell = (\mathbf{k}_\ell, i\omega_{n_\ell})$. The s-wave pair-field susceptibility $P_s(T)$ defined in Eq. (2) in the main text is then obtained from

$$P_s(T) = \frac{T}{N}\sum_{k,k'} G_{2,\uparrow\downarrow\uparrow\downarrow}(k,-k,k',-k'). \tag{A2}$$

The two-particle Green's function G_s for the lattice in the thermodynamic limit is obtained from the Bethe-Salpeter equation in the particle-particle channel shown diagrammatically in Fig. 5,

$$\begin{aligned} G_{2,\sigma_1\ldots\sigma_4}(k,-k,k',-k') = {} & G_{\sigma_1\sigma_3}(k)G_{\sigma_2\sigma_4}(-k)\delta_{k,k'} \\ & - G_{\sigma_1\sigma_4}(k)G_{\sigma_2\sigma_3}(-k)\delta_{k,-k'} \\ & + \frac{T}{N}\sum_{k''}\sum_{\sigma_5\ldots\sigma_8} G_{\sigma_1\sigma_5}(k)G_{\sigma_2\sigma_6}(-k) \\ & \times \Gamma^{pp}_{\sigma_5\ldots\sigma_8}(k,-k,k'',-k'') \\ & \times G_{2,\sigma_7\sigma_8\sigma_3\sigma_4}(k'',-k'',k',-k'). \end{aligned} \tag{A3}$$

Here, $G_{\sigma\sigma'}(k)$ is the single-particle Green's function, which, due to the Rashba spin-orbit coupling is off-diagonal in the spin, and $\Gamma^{pp}_{\sigma_4\ldots\sigma_1}(k,-k,k',-k')$ is the irreducible particle-particle vertex. In the DCA, its momentum dependence is reduced to that of the effective cluster problem, i.e., $\Gamma^{pp}_{\sigma_4\ldots\sigma_1}(k,-k,k',-k') \approx \Gamma^{pp}_{\sigma_4\ldots\sigma_1}(K,-K,K',-K')$, where $K = (\mathbf{K}, i\omega_n)$ contains the cluster momenta $\mathbf{K}$. Using the cluster vertex $\Gamma^{pp}_{\sigma_4\ldots\sigma_1}(K,-K,K',-K')$, one can then calculate the coarse-grained two-particle Green's function for the lattice,

$$\begin{aligned} &\bar{G}_{2,\sigma_1\ldots\sigma_4}(K,-K,K',-K') \\ &\equiv \frac{N_c^2}{N^2}\sum_{\mathbf{k}\in\mathcal{P}_\mathbf{K}}\sum_{\mathbf{k}'\in\mathcal{P}_{\mathbf{K}'}} G_{2,\sigma_1\ldots\sigma_4}(k,-k,k',-k') \\ &= \bar{G}^0_{2,\sigma_1\ldots\sigma_4}(K,-K,K',-K') \\ &\quad + \frac{T}{N_c}\sum_{K''}\sum_{\sigma_5\ldots\sigma_8} \bar{G}^d_{2,\sigma_1\ldots\sigma_4}(K,-K,-K,K) \\ &\quad \times \Gamma^{pp}_{\sigma_5\ldots\sigma_8}(K,-K,K'',-K'') \\ &\quad \times \bar{G}_{2,\sigma_7\sigma_8\sigma_3\sigma_4}(K'',-K'',K',-K'). \end{aligned} \tag{A4}$$

Here, the sums over $\mathbf{k}$, $\mathbf{k}'$, and $\mathbf{k}''$ have been partially carried out over the N_c DCA coarse-graining patches $\mathcal{P}_\mathbf{K}$, etc. [18], with N_c the cluster size, so that all quantities now depend on the cluster momenta $\mathbf{K}$ only. The coarse-grained bare propagators,

$$\begin{aligned} &\bar{G}^0_{2,\sigma_1\ldots\sigma_4}(K,-K,K',-K') \\ &= \frac{N_c}{N}\sum_{\mathbf{k}\in\mathcal{P}_\mathbf{K}}\left[G_{\sigma_1\sigma_3}(k)G_{\sigma_2\sigma_4}(-k)\right]\delta_{K,K'} \\ &\quad - \frac{N_c}{N}\sum_{\mathbf{k}\in\mathcal{P}_\mathbf{K}}\left[G_{\sigma_1\sigma_4}(k)G_{\sigma_2\sigma_3}(-k)\right]\delta_{K,-K'}, \end{aligned} \tag{A5}$$

and

$$\begin{aligned} &\bar{G}^d_{2,\sigma_1\ldots\sigma_4}(K,-K,K',-K') \\ &= \frac{N_c}{N}\sum_{\mathbf{k}\in\mathcal{P}_\mathbf{K}}\left[G_{\sigma_1\sigma_3}(k)G_{\sigma_2\sigma_4}(-k)\right]\delta_{K,-K'} \end{aligned} \tag{A6}$$

only has the (diagonal) first term. By including the spin variables in the combined indices $K = (\mathbf{K}, \omega_n, \sigma_1, \sigma_2)$ and $K' = (\mathbf{K}', \omega_{n'}, \sigma_3, \sigma_4)$, this equation can be conveniently written in matrix form (in K and K')

$$\bar{\mathbf{G}}_2 = \bar{\mathbf{G}}^0_2 + \bar{\mathbf{G}}^d_2\boldsymbol{\Gamma}^{pp}\bar{\mathbf{G}}_2. \tag{A7}$$

The cluster vertex $\boldsymbol{\Gamma}^{pp}$ is determined from an analogous equation for the cluster two-particle Green's function G^c_2 [18],

$$\mathbf{G}^c_2 = \mathbf{G}^{c,0}_2 + \mathbf{G}^{c,d}_2\boldsymbol{\Gamma}^{pp}\mathbf{G}^c_2. \tag{A8}$$

The bare cluster propagators

$$\begin{aligned} &G^{c,0}_{2,\sigma_1\ldots\sigma_4}(K,-K,K',-K') \\ &= G^c_{\sigma_1\sigma_3}(K)G^c_{\sigma_2\sigma_4}(-K)\delta_{K,K'} \\ &\quad - G^c_{\sigma_1\sigma_4}(K)G^c_{\sigma_2\sigma_3}(-K)\delta_{K,-K'}, \end{aligned}$$

and

$$G^{c,d}_2(K) = G^c_{\sigma_1\sigma_3}(K)G^c_{\sigma_2\sigma_4}(-K)\delta_{K,K'},$$

where $G^c_{\sigma\sigma'}(K)$ is the single-particle cluster Green's function.

The extraction of the cluster vertex $\boldsymbol{\Gamma}^{pp}$ from the Bethe-Salpeter equation (A8) involves an inversion of $\mathbf{G}^c_2$ and $\mathbf{G}^{c,0}_2$. The addition of the second term with crossed Green's function legs proportional to $\delta_{K,-K'}$ makes these matrices singular. However, after some matrix arithmetics, an equation can be

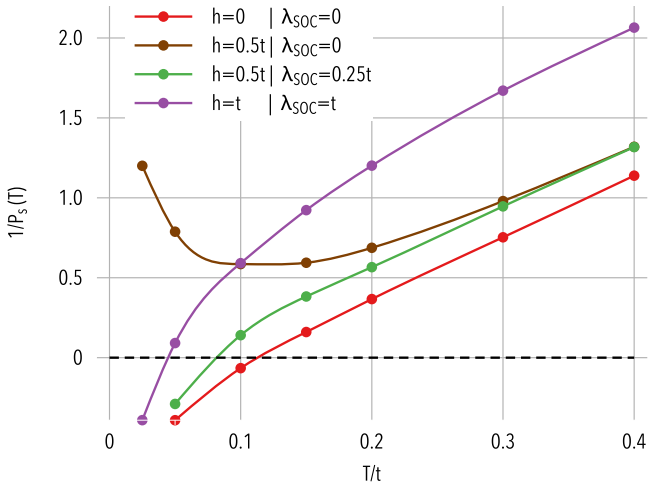

FIG. 6. Temperature dependence of inverse s-wave pair-field susceptibility. The inverse s-wave pair-field susceptibility $1/P_s(T)$ calculated according to Eq. (A10) versus temperature for different combinations of magnetic field h and Rashba spin-orbit coupling λ_{SOC}. The values for the superconducting transition temperature T_c shown in Fig. 1 in the main text are obtained from the temperature where $1/P_s(T)$ crosses zero (dashed line).

obtained for $\bar{\mathbf{G}}_2$ that does not involve the inversion of these matrices [9],

$$\bar{\mathbf{G}}_2 = \mathbf{G}_2^c\left[\left(\left[\bar{\mathbf{G}}_2^{(1)}\right]^{-1} - \left[\mathbf{G}_2^{c,(1)}\right]^{-1}\right)\mathbf{G}_2^c + \mathbf{B}^c\right]^{-1}\mathbf{B}. \quad \text{(A9)}$$

Here $\mathbf{B} = [\bar{\mathbf{G}}_2^d]^{-1}\bar{\mathbf{G}}_2^0$ and the corresponding cluster quantity $\mathbf{B}^c = [\mathbf{G}_2^{c,d}]^{-1}\mathbf{G}_2^{c,0}$. The lattice s-wave pair-field susceptibility $P_s(T)$ is then obtained from $\bar{\mathbf{G}}_2$ as

$$P_s(T) = \frac{T}{N_c}\sum_{K,K'}\bar{G}_{2,\uparrow\downarrow\uparrow\downarrow}(K,-K,K',-K'), \quad \text{(A10)}$$

and the intrinsic pair-field susceptibility $P_{s,0}(T)$ in Eq. (3) in the main text from

$$P_{s,0}(T) = \frac{T}{N_c}\sum_{K,K'}\bar{G}^0_{2,\uparrow\downarrow\uparrow\downarrow}(K,-K,K',-K'). \quad \text{(A11)}$$

The temperature dependence of the inverse of $P_s(T)$ is shown for a selected set of parameters in Fig. 6.

APPENDIX B: DENSITY MATRIX RENORMALIZATION GROUP ANALYSIS OF AN ATTRACTIVE RASHBA-HUBBARD TWO-LEG LADDER

In order to investigate the robustness of the DCA results, we also carry out complementary density matrix renormalization group (DMRG) [37,38] calculations on a two-leg ladder with open boundaries using the DMRG++ software [39], working at zero temperature. This provides accurate insight into the real-space behavior of a minimal version of the 2D problem [40,41]. We first rewrite the hopping part of Eq. (1) in real space as

$$H_0 = -t\sum_{\langle i,j\rangle,\sigma}[c^\dagger_{i\sigma}c_{j\sigma} + \mathrm{H.c.}] - h\sum_i(n_{i\uparrow} - n_{i\downarrow})$$
$$+ 2\lambda_{\mathrm{SOC}}\sum_{\langle i,j\rangle}\sum_{\sigma,\sigma'}c^\dagger_{i\sigma}\left[\alpha^x_{ij}\sigma^y_{\sigma\sigma'} - \alpha^y_{ij}\sigma^x_{\sigma\sigma'}\right]c_{j\sigma'}, \quad \text{(B1)}$$

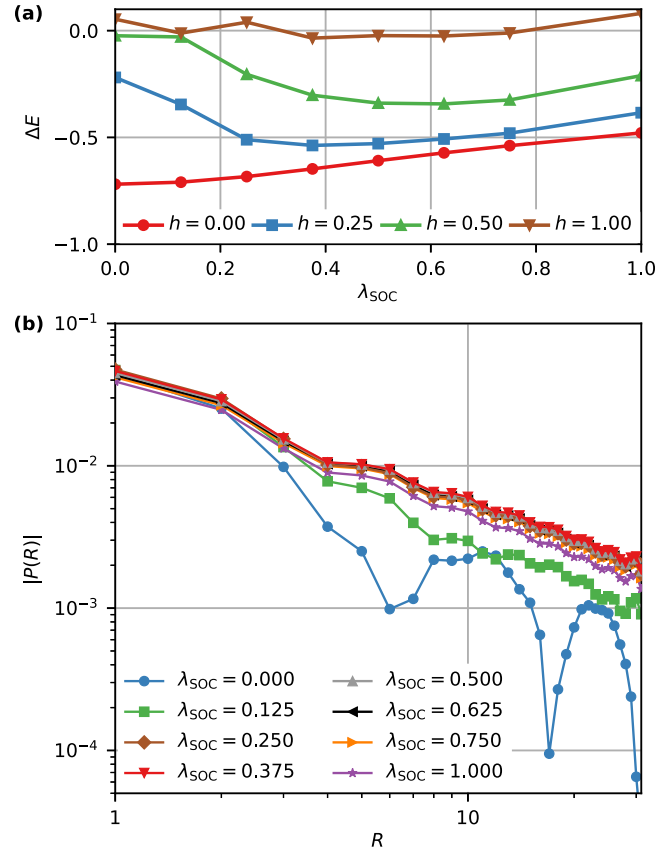

FIG. 7. Rashba-Hubbard two-leg ladder. (a) Binding energy for $L_x = 32$. (b) On-site singlet pair-pair correlations for $L_x = 48$ and $h = 0.5$. Results in both panels are obtained using DMRG for electron filling $\langle n\rangle = 0.25$ and $U = -4t$.

where $\langle\ldots\rangle$ denotes summation over nearest neighbors, $\alpha^\mu_{ij} \equiv i(\delta_{i,j+a_\mu} - \delta_{i,j-a_\mu})$, a_μ denotes translation in the μ direction [42], and we take $\hat{x}$ ($\hat{y}$) to be the long (short) direction of the ladder, namely along legs (across rungs). Here we consider ladders up to length $L_x = 48$ (and width $L_y = 2$). In obtaining the ground states, a truncation error below 10^{-9} was targeted and obtained for all parameters by keeping up to $m = 1500$ states. Explicit reorthogonalization was used at each step. The first quantity of interest is the binding energy [43],

$$\Delta E(N) = E_0(N-2) + E_0(N) - 2E_0(N-1), \quad \text{(B2)}$$

where $E_0(N)$ denotes the ground state energy of the system with N electrons present. $\Delta E(N) < 0$ indicates it is favorable for two holes to form a Cooper pair bound state, a requirement for pairing to occur. $\Delta E = 0$ for two independent holes, but $\Delta E > 0$ can also occur due to finite-size effects. The binding energy for $L_x = 32$ is plotted for several fields and λ_{SOC} values in Fig. 7(a). For intermediate fields $0.25 \leqslant h \leqslant 0.5$ we find a minimum in the binding energy at intermediate Rashba coupling, which reflects an enhanced tendency to pairing and is in qualitative agreement with the DCA results. At $h = 0.5$ the value of the binding energy only becomes appreciably negative at finite $\lambda_{\mathrm{SOC}} \geqslant 0.25$. At zero field, however, the trend is monotonous in λ_{SOC}. Some such differences between the DMRG and DCA results may be expected due to the

difference in dimensionality, but the qualitative agreement at $h = 0.5$ indicates the trend is general and robust.

We next consider pair-pair correlations for $h = 0.5$. We focus on on-site singlet pairs, which are favored by the attractive Hubbard interaction. The pair creation operator on rung i and leg a can be written $S^{\dagger}_{\mathrm{on-site}}(i) = c^{\dagger}_{ia\uparrow} c^{\dagger}_{ia\downarrow}$ and the corresponding correlation function is given by

$$P(R) = \frac{1}{N_R} \sum_i \langle S^{\dagger}_{\mathrm{on-site}}(i) S_{\mathrm{on-site}}(i+R) \rangle, \qquad \text{(B3)}$$

where N_R denotes the number of total neighbors at distance R from site i, summed over all sites. We neglect eight rungs at each end of the ladder in order to minimize edge effects. Correlations for a ladder with $L_x = 48$ are plotted in Fig. 7(b), showing power-law behavior as expected for a quasi-1D system. We see a pronounced enhancement of the correlation function upon introduction of the Rashba coupling, with a maximum near $\lambda_{\mathrm{SOC}} = 0.375$. The nonmonotonous behavior matches that of the binding energy in Fig. 7(a), and is consistent with the behavior of the s-wave intrinsic pair-field susceptibility of the 2D system shown in Fig. 3. The beneficial effect of Rashba spin mixing on singlet pairing becomes evident by comparing the correlations at finite λ_{SOC} with the much weaker correlations at $\lambda_{\mathrm{SOC}} = 0$.

[1] M. Sato and Y. Ando, Rep. Prog. Phys. **80**, 076501 (2017).
[2] X.-L. Qi and S.-C. Zhang, Rev. Mod. Phys. **83**, 1057 (2011).
[3] J. Alicea, Rep. Prog. Phys. **75**, 076501 (2012).
[4] A. Kitaev, Ann. Phys. **303**, 2 (2003).
[5] M. Sato, Y. Takahashi, and S. Fujimoto, Phys. Rev. Lett. **103**, 020401 (2009).
[6] M. Sato, Y. Takahashi, and S. Fujimoto, Phys. Rev. B **82**, 134521 (2010).
[7] J. D. Sau, R. M. Lutchyn, S. Tewari, and S. Das Sarma, Phys. Rev. Lett. **104**, 040502 (2010).
[8] S.-P. Lee, J. Alicea, and G. Refael, Phys. Rev. Lett. **109**, 126403 (2012).
[9] Y. Nagai, S. Hoshino, and Y. Ota, Phys. Rev. B **93**, 220505(R) (2016).
[10] C. Zhang, S. Tewari, R. M. Lutchyn, and S. Das Sarma, Phys. Rev. Lett. **101**, 160401 (2008).
[11] M. Sato and S. Fujimoto, Phys. Rev. Lett. **105**, 217001 (2010).
[12] A. Daido and Y. Yanase, Phys. Rev. B **94**, 054519 (2016).
[13] T. Yoshida and Y. Yanase, Phys. Rev. B **93**, 054504 (2016).
[14] X. Lu and D. Senechal, Phys. Rev. B **98**, 245118 (2018).
[15] V. Barzykin and L. P. Gor'kov, Phys. Rev. Lett. **89**, 227002 (2002).
[16] L. A. B. Olde Olthof, J. R. Weggemans, G. Kimbell, J. W. A. Robinson, and X. Montiel, Phys. Rev. B **103**, L020504 (2021).
[17] M. H. Hettler, A. N. Tahvildar-Zadeh, M. Jarrell, T. Pruschke, and H. R. Krishnamurthy, Phys. Rev. B **58**, R7475 (1998).
[18] T. A. Maier, M. Jarrell, T. Pruschke, and M. Hettler, Rev. Mod. Phys. **77**, 1027 (2005).
[19] T. A. Maier and D. J. Scalapino, Phys. Rev. B **84**, 180513(R) (2011).
[20] R. Blankenbecler, D. J. Scalapino, and R. L. Sugar, Phys. Rev. D **24**, 2278 (1981).
[21] R. T. Scalettar, E. Y. Loh, J. E. Gubernatis, A. Moreo, S. R. White, D. J. Scalapino, R. L. Sugar, and E. Dagotto, Phys. Rev. Lett. **62**, 1407 (1989).
[22] R. Micnas, J. Ranninger, and S. Robaszkiewicz, Rev. Mod. Phys. **62**, 113 (1990).
[23] A. Moreo and D. J. Scalapino, Phys. Rev. Lett. **66**, 946 (1991).
[24] J. A. Wilson, J. Phys.: Condens. Matter **13**, R945 (2001).
[25] M. Keller, W. Metzner, and U. Schollwöck, Phys. Rev. Lett. **86**, 4612 (2001).
[26] T. Paiva, R. R. dos Santos, R. T. Scalettar, and P. J. H. Denteneer, Phys. Rev. B **69**, 184501 (2004).
[27] T. Paiva, R. Scalettar, M. Randeria, and N. Trivedi, Phys. Rev. Lett. **104**, 066406 (2010).
[28] T. Kaneko and Y. Ohta, J. Phys. Soc. Jpn. **83**, 024711 (2014).
[29] P. Staar, T. Maier, and T. C. Schulthess, Phys. Rev. B **89**, 195133 (2014).
[30] R. A. Fontenele, N. C. Costa, R. R. dos Santos, and T. Paiva, Phys. Rev. B **105**, 184502 (2022).
[31] C. Wu and S.-C. Zhang, Phys. Rev. B **71**, 155115 (2005).
[32] E. Gull, P. Werner, O. Parcollet, and M. Troyer, Europhys. Lett. **82**, 57003 (2008).
[33] E. Gull, P. Staar, S. Fuchs, P. Nukala, M. S. Summers, T. Pruschke, T. Schulthess, and T. Maier, Phys. Rev. B **83**, 075122 (2011).
[34] U. R. Hähner, G. Alvarez, T. A. Maier, R. Solcà, P. Staar, M. S. Summers, and T. C. Schulthess, Comput. Phys. Commun. **246**, 106709 (2020).
[35] T. A. Maier, P. Staar, V. Mishra, U. Chatterjee, J. C. Campuzano, and D. J. Scalapino, Nat. Commun. **7**, 11875 (2016).
[36] M. Jarrell, T. Maier, C. Huscroft, and S. Moukouri, Phys. Rev. B **64**, 195130 (2001).
[37] S. R. White, Phys. Rev. Lett. **69**, 2863 (1992).
[38] S. R. White, Phys. Rev. B **48**, 10345 (1993).
[39] G. Alvarez, Comput. Phys. Commun. **180**, 1572 (2009).
[40] E. Dagotto, J. Riera, and D. Scalapino, Phys. Rev. B **45**, 5744(R) (1992).
[41] E. Dagotto and T. M. Rice, Science **271**, 618 (1996).
[42] V. Brosco and M. Capone, Phys. Rev. B **101**, 235149 (2020).
[43] E. Dagotto, Rev. Mod. Phys. **66**, 763 (1994).